

## Micropolar Fluid Poro-Elastic Squeeze Film Lubrication between a Cylinder and a Rough Flat Plate – A Special Reference to Synovial Joint Lubrication

Neminath B. Naduvinamani\* and Savitramma G. Katti

Department of Mathematics, Gulbarga University  
Gulbarga-585 106, India

\*Corresponding author: naduvinamaninb@yahoo.co.in

(Manuscript received 18 September 2013; accepted 14 January 2014; published 28 February 2014)

In the present paper the effect of micropolar squeeze film lubrication between a cylinder and a poroelastic flat plate is presented. The synovial fluid is modeled as the micropolar fluid and the articular cartilage is considered to be a poroelastic in nature. The modified averaged Reynolds equation accounting for the randomized surface roughness structure as well as elastic nature of articular cartilage with micropolar fluid as lubricant is derived. The Christensen stochastic theory for rough surfaces is used to study the effect of two types of one dimensional surface roughness on the squeeze film characteristics of a cylinder and a rough poroelastic flat plate with micropolar fluid. Results are presented for the performance of the synovial joint with the experimentally validated values of the cartilage elasticity and permeability. It is observed that, the transverse roughness pattern improves the squeeze film characteristics whereas the squeeze film bearing performance is affected due to the presence of one-dimensional longitudinal surface roughness. These effects are more pronounced for the micropolar fluids.

**Keywords:** synovial joint, surface roughness, poro-elastic, articular cartilage, micropolar fluid, squeeze film

### 1. Introduction

Human synovial joints have to withstand complex, varied and often harsh loading regimes, been subjected to both dynamic and static load under conditions of sliding and rolling [1]. The human joint is a self acting and dynamically load-bearing structure that uses a porous and elastic biomaterial as well as highly non-Newtonian lubricant for its functioning. Relative motion between two surfaces in contact is characterized by frictional forces and wear of one surface or both [2]. The friction coefficient is affected by the mechanical properties of the materials in contact; the operating conditions and the type of lubricant in the contact interface [3].

Normal synovial fluid is generally clear or yellowish and viscous. It can be briefly described as a dialysate of plasma. It contains about one third of the protein concentration of the plasma. Synovial fluid contains a very important polymer known as hyaluronic acid (mucopolysaccharide), which gives the synovial fluid its slippery and stingy behavior. It also gives it a characteristic non-Newtonian behavior. In recent years, considerable attention has been paid by researchers to the study of the mechanism of human locomotion, such as knee joints and hip joints [4].

Cartilage is basically a two-phase deformable porous

material which can be absorbed or give out fluid owing to the established pressure gradient by either squeeze film action of the synovial fluid or consolidation of the solid matrix by tissue deformation. The schematic diagram of synovial knee joint is shown in Fig. 1. The studies of Clarke [5], Mow and Lai [6] have pointed out that cartilage is a three layered porous medium consisting of a superficial tangential zone, a middle zone and a deep zone. Nigam et al. [7] investigated the effect of the variation of porosity in the upper most layer of the cartilage which according to them plays a predominant role in the self adjusting nature of the human joint, taking a three layered porous medium. Tandon and Rakesh [8]

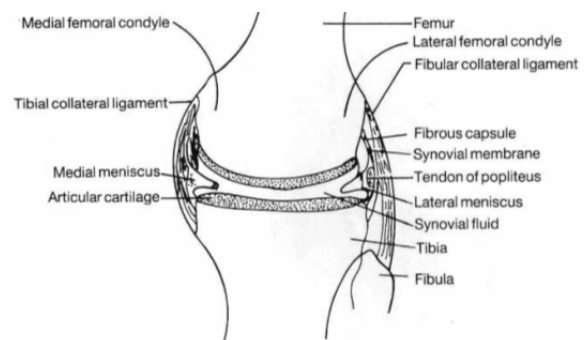


Fig. 1 A schematic diagram of a synovial knee joint

studied the lubrication mechanism occurring in knee joint replacement under restricted motion.

The squeeze film phenomena arise from the behavior of two lubricated surfaces approaching each other with a normal velocity. Since the viscous lubricant present in the film has a resistance it cannot be squeezed out instantaneously. The problem of normal approach up to spherical bodies has been studied by Christensen [9] and reported that the effect of elastic deformation profoundly influences all aspects of motion when the separation of two surfaces becomes narrow enough. Gould [10] studied the same problem by considering the lubricant to be a function of pressure and temperature and the effect of temperature on the characteristics of high pressure squeeze films has been determined. The squeeze film characteristic between a sphere and a flat plate is studied by Conway and Lee [11]. The squeeze film lubrication of micropolar fluids has been studied by many investigators (Balaram [12], Prawal Sinha [13], Zaheeruddin and Isa [14]) and observed an increased load carrying capacity and delayed time of approach.

The theoretical study of bearings has become more and more realistic due to the consideration of many physical effects such as the non-Newtonian character of the lubricants and the surface roughness effects. When the size of the surface asperity height is of the same order as that of the lubricant film thickness, one cannot neglect the surface thickness effects in the study of bearings has been sought. Consequently, an attempt has been made over the past three decades to study the effect of surface roughness on the bearing performance by using both deterministic and stochastic methods. The stochastic methods determine the gross features of a surface roughness profile. For most of the practical lubrication applications, the global mean pressure distribution is more important. The stochastic methods are best suited to characterize the surface roughness asperities effects in tribological applications. For the randomly distributed asperities Christensen [15] developed the stochastic models for hydrodynamic lubrication of rough surfaces. Prakash and Tiwari [16] developed stochastic model to study the effect of surface roughness on porous bearings on the basis of Christensen's stochastic theory. Bujurke et al. [17] studied the effect of surface roughness on squeeze film poroelastic bearings with special reference to synovial joints. Recently, Naduvinamani and Savitramma [18] studied the micropolar fluid squeeze film lubrication between rough anisotropic poroelastic rectangular plates with a special reference to synovial joint lubrication.

Many investigators recognized the random characteristic of the surface roughness and used the stochastic theory to model the surface roughness of the bearings.

The experimental results of Sayles et al. [19] revealed that cartilage surfaces are rough, and roughness height distribution is Gaussian in nature. Hence in this paper, the Christensen's stochastic theory for rough surfaces is

used to analyze the effect of surface roughness on the squeeze film characteristics of cylinder and poro-elastic flat plate with micropolar fluids. Two types of one-dimensional surface roughness (longitudinal and transverse) patterns are considered. The modified stochastic Reynolds type equation governing the mean film pressure in the presence of micropolar fluids are derived for the two types of roughness patterns. The closed form expressions for the mean film pressure, the mean load carrying capacity and squeeze film time are obtained.

## 2. Mathematical formulation of the problem

The geometry and co-ordinates of the problem are as shown in the Fig. 2. The lower surface is fixed rough poroelastic matrix. The upper surface is a rigid, long cylinder that is approaching towards the lower surface with a squeezing velocity  $V_0 \left( = \frac{\partial h}{\partial t} \right)$ . This bearing

configuration is more or less similar to squeezing action of knee joint. The lubricant in the joint cavity is taken to be Eringen's [20] micropolar fluid. The stochastic film thickness  $H$  is represented by

$$H = h(x) + h_s(x, z, \xi) \quad (1)$$

where  $h(x) \left( = h_0 + \frac{x^2}{2R} \right)$  denotes the nominal smooth part of the film geometry, while  $h_s$  is the part due to the surface asperities measured from the nominal level and is a randomly varying quantity of zero mean,  $\xi$  is an index parameter determining a definite roughness arrangement, hence for a given value of  $\xi$ , the surface component  $h_s$  of the film thickness becomes a deterministic function of the space variables.

### 2.1. Region-I (fluid film region)

The basic equations for the flow of micropolar fluid in the film region in vectorial form are

$$\frac{\partial \rho}{\partial t} + \nabla \cdot (\rho V) = 0 \quad (2)$$

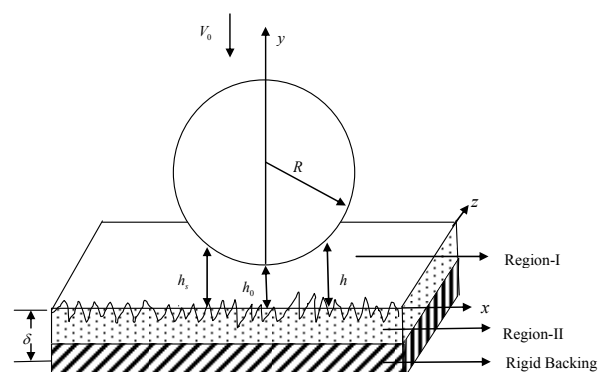


Fig. 2 Geometry of simplified model for the knee joint

$$(\lambda + 2\mu + k)\nabla(\nabla \cdot V) - (\mu + k)\nabla \times (\nabla \times V) + k\nabla \times v - \nabla \pi + \rho f \quad (3)$$

$$= \rho \left[ \frac{\partial V}{\partial t} - V \times (\nabla \times V) + \frac{1}{2} \nabla(V^2) \right] \\ (\alpha + \beta + \gamma)\nabla(\nabla \cdot V) - \gamma \nabla \times (\nabla \times V) + k\nabla \times V - 2kv + \rho l = \rho j\dot{v} \quad (4)$$

For the three dimensional steady motion of an incompressible micropolar fluid under the usual assumption of hydrodynamic lubrication with negligible body forces and body couples, the field equations (2) to (4) reduces to

**Conservation of mass**

$$\frac{\partial u}{\partial x} + \frac{\partial v}{\partial y} + \frac{\partial w}{\partial z} = 0 \quad (5)$$

**Conservation of linear momentum**

$$\left(\mu + \frac{\chi}{2}\right) \frac{\partial^2 u}{\partial y^2} + \chi \frac{\partial v_2}{\partial y} = \frac{\partial p}{\partial x}, \quad (6)$$

$$\frac{\partial p}{\partial y} = 0, \quad (7)$$

$$\left(\mu + \frac{\chi}{2}\right) \frac{\partial^2 w}{\partial y^2} + \chi \frac{\partial v_1}{\partial y} = \frac{\partial p}{\partial z}, \quad (8)$$

**Conservation of angular momentum**

$$\gamma \frac{\partial^2 v_1}{\partial y^2} - 2\chi v_1 - \chi \frac{\partial w}{\partial y} = 0, \quad (9)$$

$$\gamma \frac{\partial^2 v_2}{\partial y^2} - 2\chi v_2 - \chi \frac{\partial u}{\partial y} = 0, \quad (10)$$

where  $u$ ,  $v$  and  $w$  are velocity components along  $x$ ,  $y$  and  $z$  axes respectively and  $v_1$ ,  $v_2$  are the micropolar velocity components in the  $x$  and  $z$  directions respectively and  $p$  is the pressure in the film region.

**2.2. Region-II (poro-elastic region)**

Following Torzilli and Mow [21] and Collins [22] the coupled equations of motion for deformable cartilage matrix and the mobile portion of the fluid contained in it can be written in the form.

Matrix:

$$\rho_m \frac{\partial^2 \vec{U}}{\partial t^2} = \text{div } \tau_m - \frac{1}{k_*} \left( \frac{\partial \vec{U}}{\partial t} - \vec{V} \right) \quad (11a)$$

Fluid:

$$\rho_f \frac{D\vec{V}}{Dt} = \text{div } \tau_f + \frac{1}{k_*} \left( \frac{\partial \vec{U}}{\partial t} - \vec{V} \right) \quad (11b)$$

where  $\rho_m$  and  $\rho_f$  denote the densities of solid matrix and fluid respectively,  $\vec{U}$  is the corresponding displacement vector,  $\vec{V}$  is the fluid velocity vector,  $k_*$  is the permeability of the cartilage, and  $D/Dt$  denotes the material derivative. Equations (11a) and (11b) represent the force balance for the linear elastic solid and viscous fluid components, of the cartilage, respectively. In these equations, left hand terms denote the local forces (mass

X acceleration) which are counter balanced by right porous media driving force respectively.

In fact these two equations may be viewed simply as a generalized form of Darcy's law for unsteady flow in a deformable porous medium in terms of the relative velocity  $\left( \frac{\partial \vec{U}}{\partial t} - \vec{V} \right)$  between the moving cartilage and the fluid contained in its pores.

The classical stress tensor  $\tau$  for a continuous homogeneous medium may be expressed for the matrix and fluid, respectively as

$$\tau_m = p_1 I + N^1 e + AeI \quad (12a)$$

$$\tau_f = -p_1 I + EeI \quad (12b)$$

where  $N^1$ ,  $A$  and  $E$  are the elastic parameters of the cartilage. After neglecting the inertia terms, addition of equations (11a) and (11b) eliminate the pressure and fluid velocity and thereafter, taking the divergence of the results, yields the following Laplace equation.

$$\nabla^2 e = 0 \quad (13)$$

where  $e (= \text{div } \vec{U})$  is known as the cartilage dilatation.

Following Hori and Mockers [23] we characterize the cartilage dilatation by a sample similar linear equation in terms of corresponding average bulk modulus  $K$ , in the following form

$$e = e_0 + \frac{p_1}{K} \quad (14)$$

The equation describing pressure in the porous region is obtained by using equations (13) and (14)

$$\nabla^2 p_1 = 0 \quad (15)$$

The relevant boundary conditions for the velocity fields are

$$u = w = 0, v = -v_n, v_1 = v_2 = 0 \text{ at } y = 0, \quad (16a)$$

$$u = w = 0, v = -V_0 \left( = -\frac{\partial H}{\partial t} \right), v_1 = v_2 = 0 \text{ at } y = H \quad (16b)$$

**3. Solution of the problem**

Solving the equations (6)-(10) for the velocity components  $u$ ,  $v$  and  $w$  microrotation velocity components  $v_1$  and  $v_2$  with the respective boundary conditions given in equations (16a) and (16b) we get

$$u = \frac{1}{\mu} \left( \frac{y^2}{2} \frac{\partial p}{\partial x} + C_{11} y \right) \quad (17)$$

$$- \frac{2N^2}{m} [C_{21} \sinh(my) + C_{31} \cosh(my)] + C_{41} \\ w = \frac{1}{\mu} \left[ \frac{y^2}{2} \frac{\partial p}{\partial z} + C_{12} y \right] \quad (18) \\ - \frac{2N^2}{m} [C_{22} \sinh(my) + C_{32} \cosh(my)] + C_{42}$$

$$v_1 = -\frac{1}{2\mu} \left[ y \frac{\partial p}{\partial z} + C_{12} \right] + [C_{22} \cosh(my) + C_{32} \sinh(my)] \quad (19)$$

$$v_2 = -\frac{1}{2\mu} \left( \frac{\partial p}{\partial x} y + C_{11} \right) + [C_{21} \cosh(my) + C_{31} \sinh(my)] \quad (20)$$

where for  $i=1, 2$

$$C_{1i} = 2\mu C_{2i}$$

$$C_{2i} = \frac{C_{3i} \sinh(mh) - \frac{h}{2\mu} \frac{\partial p}{\partial x_i}}{1 - \cosh(mh)}$$

$$C_{3i} = \frac{h}{2\mu} \frac{\partial p}{\partial x_i} \times \left[ \frac{h}{2} (\cosh mh - 1) + h - \frac{N^2}{m} \sinh mh \right] \frac{1}{C_5}$$

$$C_{4i} = \frac{2N^2}{m} C_{3i}$$

$$C_5 = h \left[ \sinh(mh) - \frac{2N^2}{mh} (\cosh mh - 1) \right]$$

and  $m = \frac{N}{l}, N = \left( \frac{\chi}{2\mu + \chi} \right)^{\frac{1}{2}}, l = \left( \frac{\gamma}{4\mu} \right)^{\frac{1}{2}}$

Integrate the continuity equation (5) with respect to  $y$  over the film thickness  $H$  and using the expression (17) and (18) yields the generalized Reynolds equation is obtained in the form

$$\frac{\partial}{\partial x} \left[ f(N, l, H) \frac{\partial p}{\partial x} \right] + \frac{\partial}{\partial z} \left[ f(N, l, H) \frac{\partial p}{\partial z} \right] = -12\mu \frac{\partial H}{\partial t} + 12\mu (v_n)_{y=0} \quad (21)$$

Integrating equation (15) with respect to  $y$  in the interval  $(-\delta, 0)$  and also using the Morgan-Cameron approximation with the condition of solid backing

$$\left( \frac{\partial p_1}{\partial y} = 0 \right) \text{ at } y = -\delta \text{ we get}$$

$$\left[ \frac{\partial p_1}{\partial y} \right]_{y=0} = -\delta \left( \frac{\partial^2 p}{\partial x^2} + \frac{\partial^2 p}{\partial z^2} \right) \quad (22)$$

By neglecting inertia terms, equation (11b) may be arranged in terms of relative velocity in the form

$$\left( \vec{V} - \frac{d\vec{U}_1}{dt} \right) = -k^* (\nabla p_1 - E \nabla e) \quad (23)$$

and elimination of  $e$  through equation (15) and (23) gives

$$\left( \vec{V} - \frac{d\vec{U}_1}{dt} \right) = -k^* \nabla p_1 \left( 1 - \frac{E}{K} \right) \quad (24)$$

The normal component of the relative fluid velocity at

the cartilage surface is

$$v_n = k^* \left( \frac{E}{K} - 1 \right) \frac{\partial p_1}{\partial y} \Big|_{y=0} \quad (25)$$

By using the equation (22) in equation (25) we get

$$v_n = -k^* \delta \left( \frac{E}{K} - 1 \right) \left( \frac{\partial^2 p}{\partial x^2} + \frac{\partial^2 p}{\partial z^2} \right) \quad (26)$$

Integrating equation (5) across the fluid film and using the boundary conditions for  $v$  in equations (16a) and (16b) and also using the expression (17), (18) and (26) the modified Reynolds equation is obtained in the form

$$\frac{\partial}{\partial x} \left\{ \left[ f(N, l, H) + 12\mu k^* \delta \left( \frac{E}{K} - 1 \right) \right] \frac{\partial E(p)}{\partial x} \right\} + \frac{\partial}{\partial z} \left\{ \left[ f(N, l, H) + 12\mu k^* \delta \left( \frac{E}{K} - 1 \right) \right] \frac{\partial E(p)}{\partial z} \right\} = -12\mu \frac{\partial E(H)}{\partial t} \quad (27)$$

Taking the expectation on both sides of above equation we get, the averaged modified Reynolds equation in the form

$$\frac{\partial}{\partial x} \left\{ \left[ E \left[ f(N, l, H) \right] + 12k^* \delta \left( \frac{E}{K} - 1 \right) \right] \frac{\partial E(p)}{\partial x} \right\} + \frac{\partial}{\partial z} \left\{ \left[ E \left[ f(N, l, H) \right] + 12k^* \delta \left( \frac{E}{K} - 1 \right) \right] \frac{\partial E(p)}{\partial z} \right\} = -12\mu \frac{\partial E(H)}{\partial t} \quad (28)$$

And  $E(g) = \int_{-\infty}^{\infty} (g) f(h_s) dh_s$  (29)

where  $f(h_s)$  is the probability density function of the stochastic film thickness  $h_s$ .

In accordance with Christensen [15], we assume that

$$f(h_s) = \begin{cases} \frac{35}{32c^7} (c^2 - h_s^2)^3, & -c < h_s < c \\ 0, & \text{elsewhere} \end{cases} \quad (30)$$

In accordance with the Christensen [15] stochastic theory, the analysis is done for the two types of one-dimensional surface roughness patterns, viz., one-dimensional longitudinal roughness pattern and one-dimensional transverse roughness pattern.

For one-dimensional longitudinal roughness pattern, the roughness striations are in the form of ridges and valleys in the  $x$ -direction in this case the non-dimensional film thickness assumes the form

$$H = h(x) + h_s(z, \xi) \quad (31)$$

and the stochastic modified Reynolds (28) takes the form

$$\begin{aligned} & \frac{\partial}{\partial x} \left\{ E[f(N, l, H)] + 12\mu k^* \delta \left( \frac{E}{K} - 1 \right) \right\} \frac{\partial E(p)}{\partial x} \\ & + \frac{\partial}{\partial z} \left\{ \frac{1}{E[1/f(N, l, H)]} + 12\mu k^* \delta \left( \frac{E}{K} - 1 \right) \right\} \frac{\partial E(p)}{\partial z} \quad (32) \\ & = -12\mu \frac{\partial E(H)}{\partial t} \end{aligned}$$

For one-dimensional transverse roughness pattern, the roughness striations are in the form of ridges and valleys in the  $z$ -direction in this case the non-dimensional film thickness assumes the form

$$H = h(x) + h_s(x, \xi) \quad (33)$$

The modified Reynolds type equation (28) takes the form

$$\begin{aligned} & \frac{\partial}{\partial x} \left\{ \frac{1}{E[1/f(N, l, H)]} + 12\mu k^* \delta \left( \frac{E}{K} - 1 \right) \right\} \frac{\partial E(p)}{\partial x} \\ & + \frac{\partial}{\partial z} \left\{ E[f(N, l, H)] + 12\mu k^* \delta \left( \frac{E}{K} - 1 \right) \right\} \frac{\partial E(p)}{\partial z} \quad (34) \\ & = -12\mu \frac{\partial E(H)}{\partial t} \end{aligned}$$

For an axisymmetric case these equations reduce to

$$\begin{aligned} & \frac{\partial}{\partial x} \left\{ G(N, l, H, c) + 12k^* \delta \left( \frac{E}{K} - 1 \right) \right\} \frac{\partial E(p)}{\partial x} \\ & = -12\mu \frac{\partial E(H)}{\partial t} \quad (35) \end{aligned}$$

Where

$$G(N, l, H, c) = \begin{cases} E[f(N, l, H)] & \text{for longitudinal roughness} \\ E\left[\frac{1}{f(N, l, H)}\right]^{-1} & \text{for transverse roughness} \end{cases}$$

$$E[f(N, l, H)] = \frac{35}{32c^7} \int_{-c}^c f(N, l, H) (c^2 - h_s^2)^3 dh_s$$

$$E[1/f(N, l, H)] = \frac{35}{32c^7} \int_{-c}^c \frac{1}{f(N, l, H)} (c^2 - h_s^2)^3 dh_s$$

$$E(H) = h$$

The relevant boundary conditions are

$$p = 0 \quad \text{at } x = L \quad (36a)$$

$$\frac{dE(p)}{dx} = 0 \quad \text{at } x = 0 \quad (36b)$$

Integrating the stochastic Reynolds type equation with respect to  $x$  and using the boundary condition (36a) and (36b) we get

$$E(p) = - \int_x^L \frac{12\mu x (\partial h / \partial t)}{\left[ G(N, l, H, c) + 12k^* \delta \left( \frac{E}{K} - 1 \right) \right]} dx \quad (37)$$

Introducing the following non-dimensional variables and parameter

$$\begin{aligned} \bar{x} &= \frac{x}{L}, \quad \bar{l} = \frac{l}{h_0}, \quad \bar{k} = \frac{k^*}{h_0^2}, \quad \bar{\delta} = \frac{\delta}{h_0}, \\ \bar{P} &= \frac{E(p)h_0^2}{\mu L (\partial h / \partial t)}, \quad \psi \left( = \frac{k^* \delta}{h_0^3} \right), \quad c = \frac{c}{h_0}, \\ \bar{H} &= \frac{H}{h_0} = \bar{h} + \bar{h}_s = \frac{h}{h_0} + \frac{h_s}{h_0} = 1 + \frac{\bar{x}^2}{2\varepsilon} + \bar{h}_s \end{aligned}$$

with  $\varepsilon = \frac{h_0}{L}$

In to the above equation, we get the non-dimensional modified Reynolds type equation in the form

$$\begin{aligned} \bar{P} &= - \frac{E(p)h_0^2}{\mu L (\partial h / \partial t)} \\ &= \int_{\bar{x}}^1 \frac{12\bar{x}}{G(N, \bar{l}, \bar{H}, \bar{c}) + 12\bar{k}\bar{\delta} \left( \frac{E}{K} - 1 \right)} d\bar{x} \quad (38) \end{aligned}$$

The mean load carrying capacity  $E(W)$  is given by

$$E(W) = \int_{-L}^L E[p(x)] dx \quad (39)$$

The non-dimensional load carrying capacity is obtained as

$$\begin{aligned} \bar{W} &= - \frac{h_0^2 E(W)}{\mu (\partial h / \partial t) L^2} \\ &= \int_{-1}^1 \int_{\bar{x}}^1 \frac{12\bar{x}}{\left[ G(N, \bar{l}, \bar{H}, \bar{c}) + 12\bar{k}\bar{\delta} \left( \frac{E}{K} - 1 \right) \right]} d\bar{x} \quad (40) \end{aligned}$$

For any given constant load, the time-height relation in dimensionless form is obtained as

$$\bar{T} = - \frac{E(W)h_0^2 t}{\mu L^2} = \int_{h_0}^1 \frac{12}{\bar{W}} d\bar{h} \quad (41)$$

#### 4. Results and discussion

The effect of surface roughness pattern on the squeeze film characteristics of a cylinder and a poro-elastic flat plate lubricated with micropolar fluids are obtained for different values of various non-dimensional parameters such as coupling number,

$$N \left( = \frac{\chi}{\chi + 2\mu} \right)^{1/2} \text{ the parameter, } \bar{l} \left( = \frac{l}{h_0} \right)$$

characterizes the interaction of the bearing geometry with the lubricant properties. In the limiting case as  $\bar{l} \rightarrow 0$  the effect of microstructures becomes negligible. The effect of permeability is observed through the non-dimensional permeability parameter,  $\psi \left( = \frac{k^* \delta}{h_0^3} \right)$  and it is to be noted

that as  $\psi \rightarrow 0$  the problem reduces to the corresponding solid case.

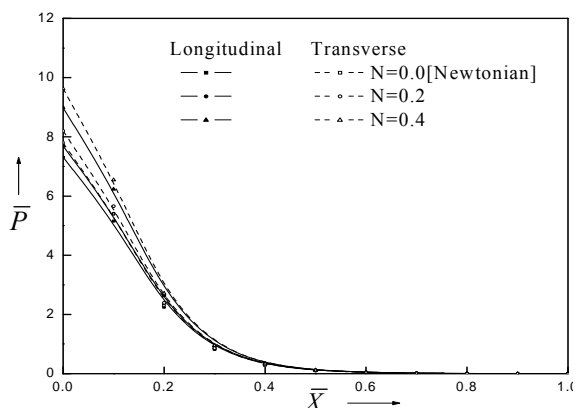


Fig. 3 Variation of non-dimensional squeeze film pressure  $\bar{P}$  with  $\bar{X}$  for different values of  $N$  with  $\bar{l} = 0.2$ ,  $E/K = 0.3$ ,  $\bar{c} = 0.2$ ,  $\bar{k} = 7.65 \times 10^{-5}$  and  $\bar{\delta} = 300$

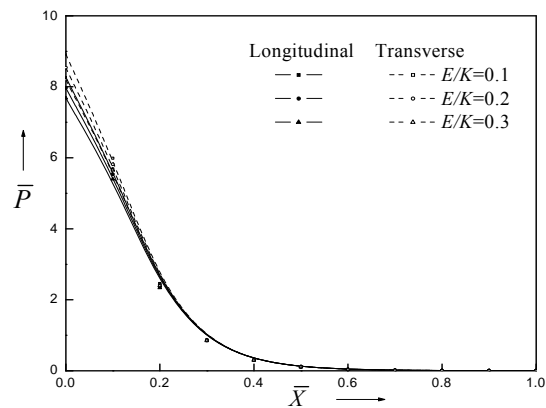


Fig. 5 Variation of non-dimensional squeeze film pressure  $\bar{P}$  with  $\bar{X}$  for different values of  $E/K$  with  $N=0.2$ ,  $\bar{l} = 0.2$ ,  $\bar{c} = 0.2$ ,  $\bar{k} = 7.65 \times 10^{-5}$  and  $\bar{\delta} = 300$

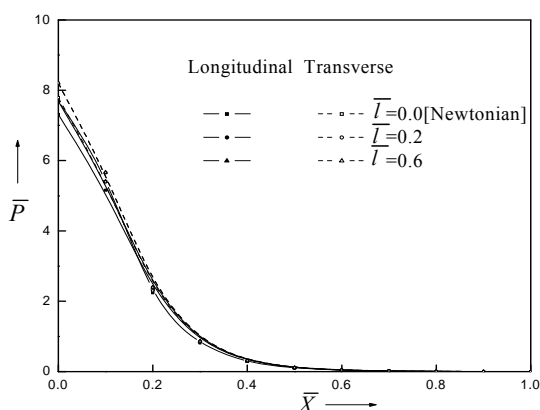


Fig. 4 Variation of non-dimensional squeeze film pressure  $\bar{P}$  with  $\bar{X}$  for different values of  $\bar{l}$  with  $N = 0.2$ ,  $E/K = 0.3$ ,  $\bar{c} = 0.2$ ,  $\bar{k} = 7.65 \times 10^{-5}$  and  $\bar{\delta} = 300$

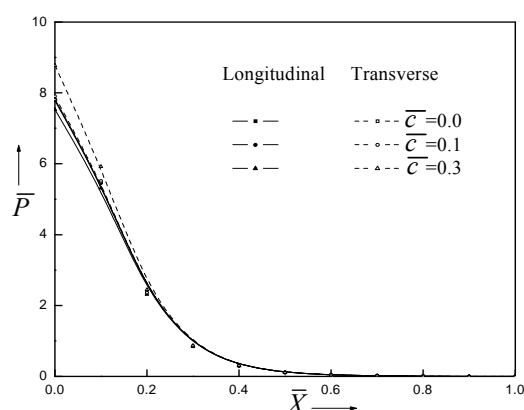


Fig. 6 Variation of non-dimensional squeeze film pressure  $\bar{P}$  with  $\bar{X}$  for different values of  $\bar{c}$  with  $N = 0.2$ ,  $E/K = 0.3$ ,  $\bar{l} = 0.2$ ,  $\bar{k} = 7.65 \times 10^{-5}$  and  $\bar{\delta} = 300$

The effect of surface roughness is characterized by the roughness parameter  $\bar{c} \left( = \frac{c}{h_0} \right)$  and it is to be noted that as  $\bar{c} \rightarrow 0$  the problem reduces to the corresponding smooth case and as  $\bar{l}, N \rightarrow 0$  it reduces to the corresponding Newtonian case.

#### 4.1. Squeeze film pressure

The variation of non-dimensional squeeze film pressure  $\bar{P}$  with  $\bar{X}$  for different values of  $N$  as a function is shown in Fig. 3 with the parameter values of  $\bar{l} = 0.2$ ,  $E/K = 0.3$ ,  $\bar{c} = 0.3$ ,  $\bar{k} = 7.65 \times 10^{-5}$  and  $\bar{\delta} = 300$  for both types of roughness pattern. It is observed that, the effect of  $N$  is to increase  $\bar{P}$  in either case as compared to the Newtonian case. Further the increase in  $\bar{P}$  is more pronounced for the transverse roughness pattern as compared to the longitudinal roughness pattern. Fig. 4 shows the variation  $\bar{P}$  with  $\bar{X}$  for different

values of  $\bar{l}$  with  $N = 0.2$ ,  $E/K = 0.3$ ,  $\bar{c} = 0.3$ ,  $\bar{k} = 7.65 \times 10^{-5}$  and  $\bar{\delta} = 300$  for both types of roughness patterns. It is observed that, the effect of  $\bar{l}$  is to increase  $\bar{P}$  in either cases as compared to the Newtonian case. Further the increase in  $\bar{P}$  is more pronounced for the transverse roughness pattern as compared to the longitudinal roughness pattern.

Fig. 5 shows the variation of  $\bar{P}$  with  $\bar{X}$  for different values of  $E/K$  with  $N = 0.2$ ,  $\bar{l} = 0.2$ ,  $\bar{c} = 0.3$ ,  $\bar{k} = 7.65 \times 10^{-5}$  and  $\bar{\delta} = 300$  for both types of roughness patterns. It is observed that,  $\bar{P}$  increases with  $\bar{X}$  and decreases for increasing values of  $E/K$  for both the types of roughness pattern. Further the increase in  $\bar{P}$  is more pronounced for the transverse roughness pattern as compared to the longitudinal roughness pattern. The variation of non-dimensional film pressure  $\bar{P}$  with  $\bar{X}$  for different values of roughness parameter  $\bar{c}$  as a

function is shown in the Fig. 6 with the parameter values of  $\bar{l}$  for both types of roughness patterns. It is observed that,  $\bar{P}$  increases (decreases) as  $\bar{c}$  increases for transverse (longitudinal) roughness pattern.

#### 4.2. Load carrying capacity

The variation of non-dimensional load  $\bar{W}$  with  $N$  for different values of  $\bar{l}$  as a function with the parameter values of  $E/K = 0.3$ ,  $\bar{c} = 0.3$ ,  $\bar{k} = 7.65 \times 10^{-5}$  and  $\bar{\delta} = 300$  is shown in the Fig. 7 it is observed that,  $\bar{W}$  increases for the increasing values of  $N$  and this increase is more accentuated for larger of  $\bar{l}$  both types of roughness pattern. Further the increase in  $\bar{W}$  is more pronounced for the transverse roughness pattern as compared to the longitudinal roughness pattern. Fig. 8 shows the variation of non-dimensional load  $\bar{W}$  with  $N$  for different values of  $E/K$  with  $\bar{l} = 0.2$ ,  $\bar{c} = 0.3$ ,  $\bar{k} = 7.65 \times 10^{-5}$  and  $\bar{\delta} = 300$  for both types of roughness

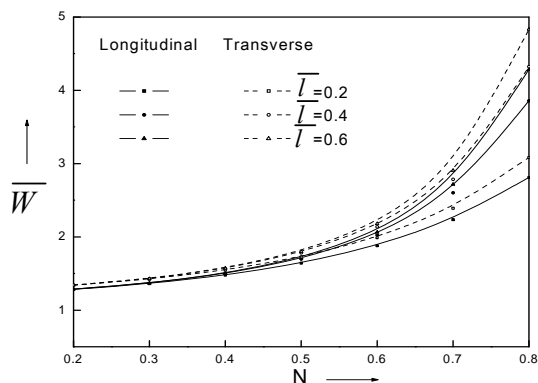


Fig. 7 Variation of non-dimensional load carrying capacity  $\bar{W}$  with  $N$  for different values of  $\bar{l}$  with  $E/K = 0.3$ ,  $\bar{c} = 0.2$ ,  $\bar{k} = 7.65 \times 10^{-5}$  and  $\bar{\delta} = 300$

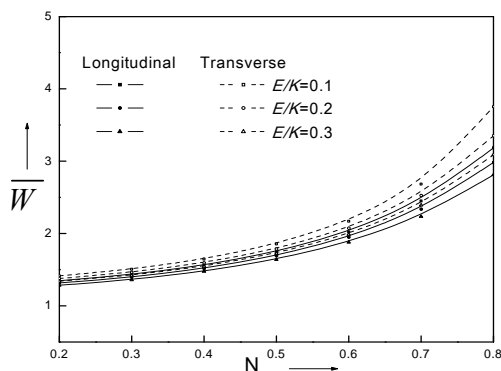


Fig. 8 Variation of non-dimensional load carrying capacity  $\bar{W}$  with  $N$  for different values of  $E/K$  with  $\bar{l} = 0.2$ ,  $\bar{c} = 0.3$ ,  $\bar{k} = 7.65 \times 10^{-5}$  and  $\bar{\delta} = 300$

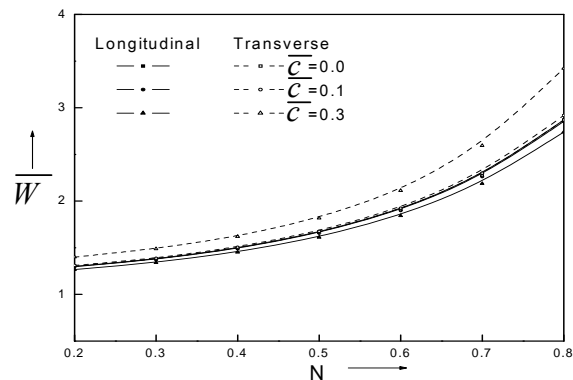


Fig. 9 Variation of non-dimensional load carrying capacity  $\bar{W}$  with  $N$  for different values of  $\bar{c}$  with  $E/K = 0.3$ ,  $\bar{l} = 0.2$ ,  $\bar{k} = 7.65 \times 10^{-5}$  and  $\bar{\delta} = 300$

patterns. It is observed that,  $\bar{W}$  increases with  $N$  and decreases for increasing values of  $E/K$  for both the types of roughness pattern. Further the increase in  $\bar{P}$  is more pronounced for the transverse roughness pattern as compared to the longitudinal roughness pattern. The variation of non-dimensional load  $\bar{W}$  with  $N$  for different values of roughness parameter  $\bar{c}$  as a function is shown in the Fig. 9 with the parameter values of  $E/K = 0.3$ ,  $\bar{l} = 0.2$ ,  $\bar{k} = 7.65 \times 10^{-5}$  and  $\bar{\delta} = 300$  for both types of roughness patterns. It is observed that,  $\bar{P}$  increases (or decreases) as  $\bar{c}$  increases for transverse (or longitudinal) roughness pattern.

#### 4.3. Squeeze film time

The variation of non-dimensional squeeze film time  $\bar{T}$  with  $\bar{h}_0$  for different values of  $N$  as a function is shown in Fig. 10 with the parameter values of  $\bar{l} = 0.2$ ,  $E/K = 0.3$ ,  $\bar{c} = 0.3$ ,  $\bar{k} = 7.65 \times 10^{-5}$  and  $\bar{\delta} = 300$  for both types of roughness pattern. It is observed that,  $\bar{T}$  increases for the decreasing values of  $N$  for both the types roughness pattern. Further the increase in  $\bar{T}$  is more pronounced for the transverse roughness pattern as compared to the longitudinal roughness pattern. The variation of non-dimensional squeeze film time  $\bar{T}$  with  $\bar{h}_0$  for different values of  $\bar{l}$  as a function is shown in Fig. 11 with the parameter values of  $N = 0.2$ ,  $E/K = 0.3$ ,  $\bar{c} = 0.3$ ,  $\bar{k} = 7.65 \times 10^{-5}$  and  $\bar{\delta} = 300$  for both types of roughness pattern. It is observed that,  $\bar{T}$  increases for the decreasing values of  $\bar{l}$  for both the types roughness pattern. Further the increase in  $\bar{T}$  is more pronounced for the transverse roughness pattern as compared to the longitudinal roughness pattern. Fig. 12 shows the variation of non-dimensional squeeze film time  $\bar{T}$  with  $\bar{h}_0$  for different values of  $E/K$  with  $N = 0.2$ ,  $\bar{l} = 0.2$ ,  $\bar{c} =$

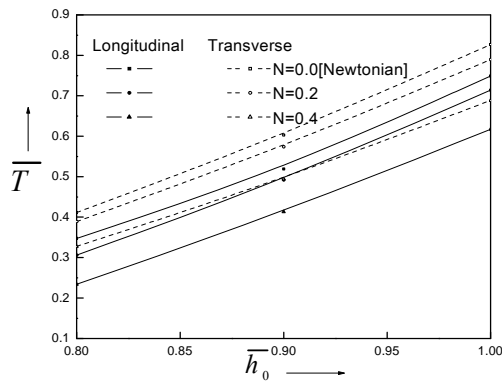


Fig. 10 Variation of non-dimensional squeeze film time  $\bar{T}$  with  $\bar{h}_0$  for different values of  $N$  with  $E/K = 0.3$ ,  $\bar{l} = 0.2$ ,  $\bar{c} = 0.3$ ,  $\bar{k} = 7.65 \times 10^{-5}$  and  $\bar{\delta} = 300$

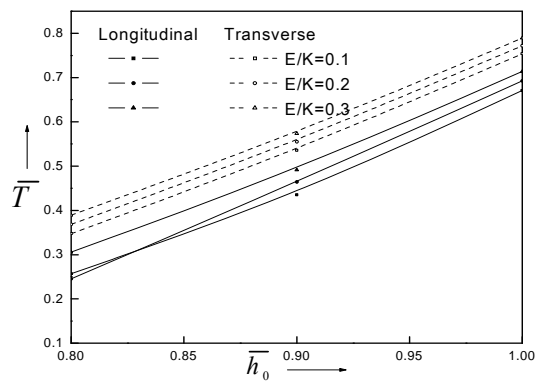


Fig. 12 Variation of non-dimensional squeeze film time  $\bar{T}$  with  $\bar{h}_0$  for different values of  $E/K$  with  $N = 0.2$ ,  $\bar{l} = 0.2$ ,  $\bar{c} = 0.3$ ,  $\bar{k} = 7.65 \times 10^{-5}$  and  $\bar{\delta} = 300$

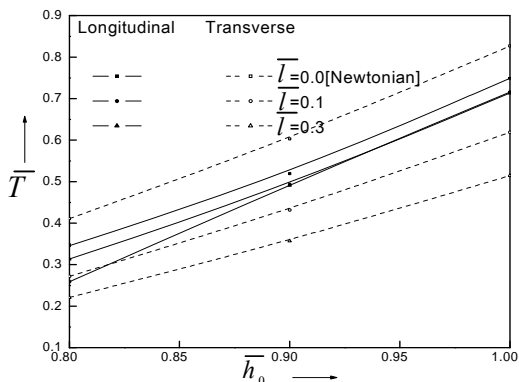


Fig. 11 Variation of non-dimensional squeeze film time  $\bar{T}$  with  $\bar{h}_0$  for different values of  $\bar{l}$  with  $E/K = 0.3$ ,  $N = 0.2$ ,  $\bar{c} = 0.3$ ,  $\bar{k} = 7.65 \times 10^{-5}$  and  $\bar{\delta} = 300$

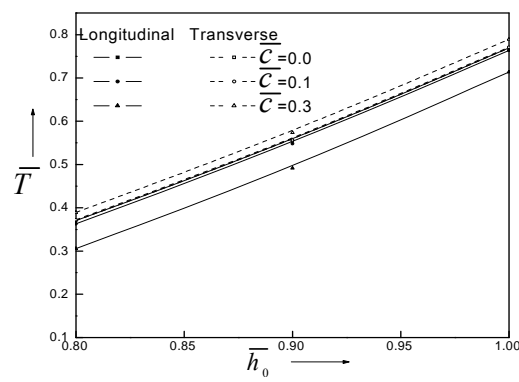


Fig. 13 Variation of non-dimensional squeeze film time  $\bar{T}$  with  $\bar{h}_0$  for different values of  $\bar{c}$  with  $E/K = 0.3$ ,  $\bar{l} = 0.2$ ,  $N = 0.2$ ,  $\bar{k} = 7.65 \times 10^{-5}$  and  $\bar{\delta} = 300$

0.3,  $\bar{k} = 7.65 \times 10^{-5}$  and  $\bar{\delta} = 300$  for both types of roughness patterns. It is observed that,  $\bar{T}$  increases with  $\bar{h}_0$  and increases for increasing values of  $E/K$  for both the types of roughness pattern. Further the increase in  $\bar{T}$  is more pronounced for the transverse roughness pattern as compared to the longitudinal roughness pattern. The variation of non-dimensional squeeze film time  $\bar{T}$  with  $\bar{h}_0$  for different values of roughness parameter  $\bar{c}$  as a function is shown in the Fig. 13 with the parameter values of  $N = 0.2$ ,  $E/K = 0.3$ ,  $\bar{l} = 0.2$ ,  $\bar{k} = 7.65 \times 10^{-5}$  and  $\bar{\delta} = 300$  for both types of roughness patterns. It is interesting to note that the effect of  $\bar{c}$  is to increase (or decrease) the response time of the squeeze film for the transverse (or longitudinal) roughness pattern, as compared to the corresponding smooth case.

### 5. Conclusions

On the basis of Eringen's micropolar fluid theory and Christensen's stochastic theory for rough surfaces, this paper predicts the effect of micropolar on the squeeze film characteristics of cylinder and a poro-elastic flat plate. The following conclusions can be drawn on the basis of the results and discussion

1. The presence of the microstructure additives in the lubricants enhances the load carrying capacity and squeeze film time as compared to the corresponding Newtonian case.
2. The presence of one-dimensional Transverse (longitudinal) roughness pattern on the poro-elastic flat plate increases (decreases) the load carrying capacity and the squeeze film time as compared to the corresponding smooth case.
3. The poro-elastic nature of cartilage reduces to the load carrying capacity and increases the squeeze film time for increasing values of the

permeability and reverse trend is observed for the increasing values of the elastic parameter.

### Acknowledgment

One of the authors Savitramma G K sincerely acknowledges the financial assistance of University Grants Commission (UGC), New Delhi under BSR Research Fellowship in Science for Meritorious Students (RFSMS).

### Nomenclature

$e$	cartilage dilatation
$E$	Expectancy operator
$E/K$	Elastic parameter
$c$	Roughness parameter
$\bar{c}$	Non-dimensional roughness parameter
$h$	Film thickness measured between the nominal mean levels of the bearing surfaces. $\left( = h_0 + \frac{x^2}{2R} \right)$
$h_0$	Initial minimum film thickness
$\bar{h}$	Non-dimensional nominal film thickness $\left( = \frac{h}{h_0} \right)$
$K$	cartilage bulk modulus
$k^*$	Cartilage permeability
$\bar{k}$	Non-dimensional permeability ( $=k^*/h_0^2$ )
$L$	characteristic length
$l$	Characteristic length of the polar suspension $\left( = \left( \frac{\gamma}{4\mu} \right)^{1/2} \right)$
$\bar{l}$	Non-dimensional form of $l$ $\left( = \frac{l}{h_0} \right)$
$N$	Coupling number $\left( = \left\{ \frac{\chi}{(2\mu + \chi)} \right\}^{1/2} \right)$
$p$	Fluid film pressure
$\bar{P}$	Non-dimensional fluid film pressure
$p_1$	Pressure in the porous region
$R$	Radius of the cylinder
$t$	Squeeze film time
$\bar{T}$	Non-dimensional squeeze film time $\left( = \frac{E(W)h_0^2t}{\mu L^2} \right)$
$\bar{U}$	Displacement vector
$\bar{V}$	Fluid velocity vector in the porous region
$u, v, w$	Velocity components in the film region
$V_0$	Approach velocity ( $=dH/dt$ )
$v_n$	Normal component of relative velocity

$v_1, v_2$	Microrotation velocity components
$W$	Load carrying capacity
$\bar{W}$	Non-dimensional load carrying capacity $\left( = \frac{h_0^2 E(W)}{\mu(\partial h / \partial t)L^2} \right)$
$x, y, z$	Cartesian co-ordinates
$\gamma$	Viscosity coefficient for micropolar fluids
$\mu$	Classical viscosity coefficients
$\rho$	Density
$\delta$	Cartilage thickness
$\bar{\delta}$	Non-dimensional cartilage thickness ( $=\delta/h_0$ )
$\chi$	Spin viscosity coefficient

### References

- [1] Stachowiack, G. W., Batchelor, A. W. and Griffiths, L. J., "Friction and wear changes in synovial joints," *Wear*, 171, 1994, 135-142.
- [2] Mow, V. C. and Ateshian, G. A., "Friction, Lubrication, and Wear of Diarthrodial Joints. In: Basic Orthopedic Biomechanics", V. C. Mow and W. C. Hayes (eds), Raven Press, New York, 2nd ed, 1997, 275-315.
- [3] Furey, M., "Joint lubrication", *The Biomedical Engineering Handbook* (Bronzino, J. D., ed.), CRC Press, Boca Raton, 2000, 21-26.
- [4] Sambasiva Rao, P., Srivathsa, B. and Murthy, P.N., "A Numerical Scheme for Hydrodynamic Lubrication of Synovial Fluid," *Indian J. Pure Appl. Math*, 26, 8, 1995, 831-835.
- [5] Clarke, I. C., "Articular Cartilage: A Review and Scanning Electron Microscope Study: 1.The Interterritorial Fibrillar Architecture," *J. Bone. Jt. Surg. Br.*, 53, 4, 1971, 732-750.
- [6] Mow, V. C. and Lai, W. M., "Some Surface Characteristics of Articular Cartilage. I. A Scanning Electron Microscopy Study and a Theoretical Model for the Dynamic Interaction of Synovial Fluid and Articular Cartilage," *J. Biomech.* 7, 5, 1974, 449-456.
- [7] Nigam, K. M., Manohar, K. and Jaggi, S., "Micropolar Fluid Film Lubrication between Two Parallel Plates with Reference to Human Joints," *Int J. Mech. Sci.* 24, 11, 1982, 661-671.
- [8] Tandon, P. N. and Rakesh, L., "A Model for Lubrication Mechanism in Knee Joint Replacement," *Def. Sci. J.* 36, 1, 1986, 45-56.
- [9] Christensen, H., "Elastohydrodynamic Theory of Spherical Bodies in Normal Approach," *ASME J. Lubr. Tech*, 92, 1, 1970, 145-154.
- [10] Gould, P., "High-Pressure Spherical Squeeze Films," *ASME J. Lubr. Tech*, 92, 1971, 207-208.
- [11] Conway, D. and Lee, H. C., "Impact of a Lubricated Surface by a sphere," *ASME J. Lubr. Tech*, 97, 1975, 613-615.
- [12] Balaram, M., "Micropolar Squeeze Film," *ASME J. Lubr. Tech*, 1975, 635-637.

- [13] Prawal S., "Dynamically Loaded Micropolar Fluid Lubricated Journal Bearings with Special Reference to Squeeze Films under Fluctuating Loads," *Wear*, 45, 3, 1977, 279-292.
- [14] Zaheeruddin, K. H. and Isa, M., "Characteristics of Micropolar Lubricant in a Squeeze Film Porous Spherical Bearings," *Wear*, 51, 1, 1978, 1-10.
- [15] Christensen, H., "Stochastic models of hydrodynamic lubrication of rough surfaces," *Proc. Inst. Mech. Eng. (Part J)* 184, 55, 1969, 1013-1026.
- [16] Prakash, J. and Tiwari, K., "Lubrication of Porous Bearing with Surface Corrugations," *J. Lub. Techn.*, 104, 1, 1982, 127-134.
- [17] Bujurke, N. M., Kudenatti R. B. and Awati V. B., "Effect of Surface roughness on Squeeze Film Poroelastic Bearings with Special Reference to Synovial Joints," *Math. Bioscis.*, 209, 1, 76-89, 2007.
- [18] Naduvinamani, N. B. and Savitramma G. K., "Micropolar Fluid Squeeze Film Lubrication between Rough Anisotropic Poroelastic Rectangular Plates: Special Reference to Synovial Joint Lubrication," *Tribology-, Mat., Surf. and Interfaces*, 6, 4, 2012, 174-181.
- [19] Sayles, R. S., Thomas, T. R., Anderson, J., Haslock, I. and Unsworth, A., "Measurement of Surface Microgeometry of Articular Cartilage," *J. Biomech.*, 12, 4, 1979, 257-267.
- [20] Eringen, A. C., "Theory of Micropolar Fluids," *J. Math. and Mech.*, 16, 1966, 1-18.
- [21] Torzilli, P. A. and Mow, V. C., "On the Fundamental Fluid Transport Mechanisms Through Normal and Pathological Articular Cartilage during Function-II," *J. Biomech.* 9, 9, 1976, 587-606.
- [22] Collins, R. J., "A Model of Lubricant Gelling in Synovial Joints," *ZAMP*, 33, 1, 1982, 93-123.
- [23] Hori, R. Y., and Mockros, L. F., "Indentation Tests of Human Articular Cartilage," *J. Biomech.* 9, 4, 1976, 259-268.